AI-Based Mathematical Modeling and Simulation of Thermal Effects in Lubrication of Rolling/Sliding Contacts

Bhupal Kumar[1*], Bimal Kumar[2], Ashish Narayan[3] and Ayani Nandi[4]

[1*]Department of Mechanical Engineering, Government Engineering College
Jamui, Bihar, India
Corresponding author's email: kbhupal246 [AT] gmail.com

[2]Department of Civil Engineering, Government Engineering College
Jamui, Bihar, India

[3]Department of Mechanical Engineering, Ramgarh Engineering College
Ramgarh, India
Email: ashishnarayan2007 [AT] gmail.com

[4]Department of Electronics and Communication Engineering, Ramgarh Engineering College,
Ramgarh, India

ABSTRACT— *In this study, we investigated the thermal effects of non-Newtonian fluids in the lubrication of rollers under rolling or sliding contacts, considering both uniform and non-uniform conditions using advanced AI-based mathematical tools. Our findings indicate that temperature influences stability by slightly shifting the position of the pressure peak away from the center line of the contact. Despite this shift, the pressure peak consistently appears near the exit of the film, regardless of thermal effects. Additionally, the squeezing motion of the surfaces significantly impacts the pressure peak, with both cavitation pressure and temperature increasing as the squeezing velocity decreases.*

Keywords- Modeling, Lubrication, bearing, hydrodynamics, non-Newtonian fluids

1. INTRODUCTION

Tribology deals with the study of interacting surfaces in relative motion, while a bearing is a mechanical component used to prevent its motion in the direction of an applied load while at the same time allowing motion in the other specified direction. Since there is an interaction between the surfaces during the process of sliding, rolling, etc., some of the supplied energy is lost due to unwanted frictional forces opposing the motion. Lubrication technology is a practice of controlling these unwanted forces, reducing wear, deformation, etc. by introducing some type of material into relative motion between these interacting surfaces. Imposing of such substance between the mating surfaces make them operate more efficiently. This substance is called a lubricant. The most commonly used lubricants are oils and greases.

Considering power law lubricants most of the articles of roller bearings i.e. pure rolling motion have been studied using symmetric conditions, i.e. both rollers have the same dimensions and velocity [1-6]; Symmetric conditions for pure rolling were also created in all previous research. Specifically, the lubricant flow was made symmetric about the X-axis. How true these ideal symmetric conditions are under actual operation is a matter of fact to be investigated. An obvious generalization of the work presented earlier would be the relaxation of the symmetric conditions i.e. the two rollers can be assumed to have different shape and sizes as well velocities (the anti-symmetric case). This is how rolling/sliding operations come into picture. Many researchers have worked on the field of sliding contacts. Few of them are included in this part. Keeping temperature and pressure dependent viscosity the Reynolds equation has been formulated. Some people solved this equation using approximation method. In this work, the transient heat transfer distribution of dry rolling contact was discussed. In between the contact, the pressure of non-Newtonian trends of lubricants was discussed. It is generally happening due to generation of high pressure and shear stress for very small fraction of time in the vicinity, resulting non-Newtonian behavior shows. In addition to that in that vicinity due to the generation of high pressure and temperature with high velocity is the important factor of damage. Bush et al [7] used surface roughness effects to study the rolling line contact behavior. Apart from this it also includes power law and sinh law. Numerical and experimental result was indicated clearly for comparing them. The variation of temperature and pressure on Newtonian and influence of temperature and pressure were discussed properly.

Anti-symmetric conditions have been used in most of the references cited above. Obviously, it is clear that during rolling/sliding concentrated contacts the lubricant properties change with pressure and temperature. Specially, the lubricant-viscosity changes significantly. In general, non-Newtonian characteristic of the lubricant used in roller seems to be important. Generally the lubricant pressure and temperature in case of rolling/sliding are expected to be higher than

those for the pure rolling case; it becomes far important to incorporate the non-Newtonian behavior of the lubricant together with variable viscosity.

The present work deals with the cylindrical rollers using variable velocity and variable dimension. The power law used to analysis of fluid film lubrication under cavitation's boundary conditions. For mathematical simulation planner geometry has been used. Linear pattern has been shown by the lubricant. The mass of lubricant is very small it can be ignored due to easy in solution. It also reduces the calculation time. To identify the -ve and +ve velocity gradient profile very straight and simple method is adopted.

2. MODELING AND SIMULATION

The proper equation with proper notation has been used, in which the two rollers are assumed to have different dimension and velocities, are

$$\frac{dp}{dX}=\frac{\partial\left(m\left|\frac{\partial u}{\partial Y}\right|^{n-1}\frac{\partial u}{\partial Y}\right)}{\partial Y} \tag{1}$$

$$\frac{\partial u}{dX}+\frac{\partial v}{dY}=0 \tag{2}$$

where m follows the relation (2.2)

$$m=m_o e^{\alpha p-\beta(T_m-T_o)} \tag{3}$$

with

$$T_m=\frac{1}{h}\int_0^h T dy \tag{4}$$

From the point of view of mathematical analysis, the contact between two cylinders of radii R_a and R_b, as shown in Fig. 1(a) can be described by an equivalent cylinder near a plane, shown in Fig. 1(b)) [8].

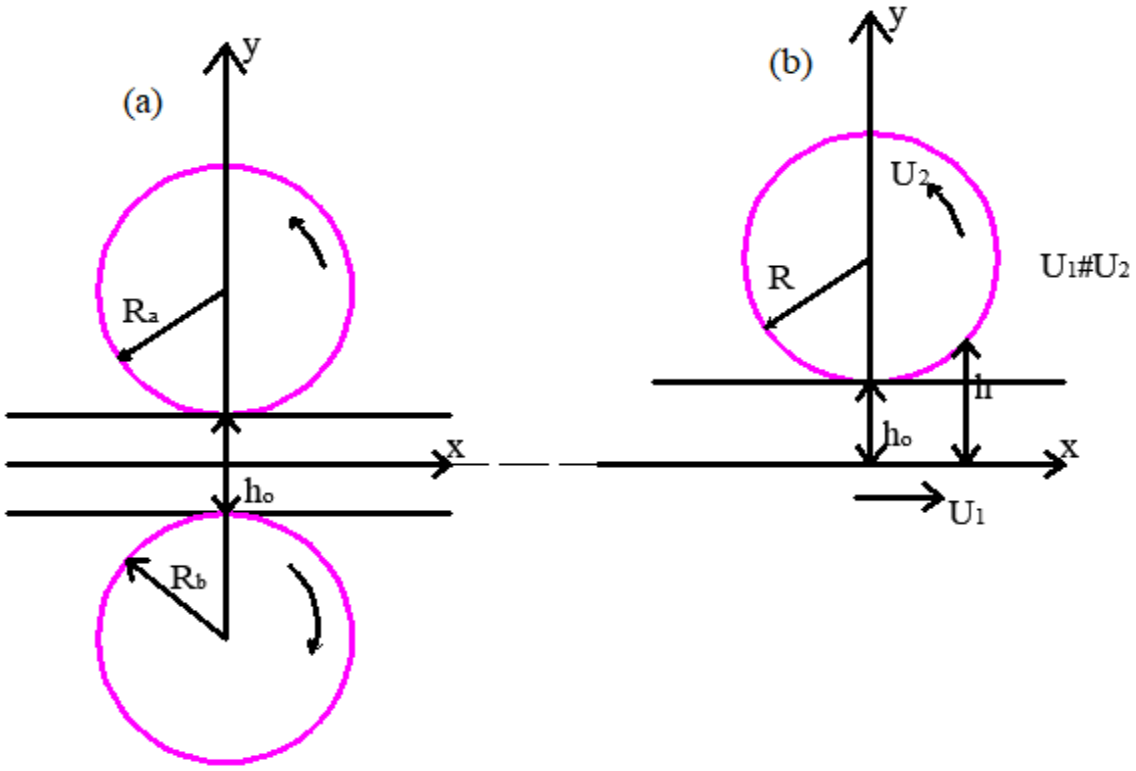

Fig. 1 (a) Lubrication of two cylindrical rollers having different dimensions and velocities Fig. 1 (b) Lubrication of a cylindrical on a plane

Film thickness h for the geometry given in Fig. 1 (b) is expressed as

$$h = h_o + \frac{X^2}{2R} \tag{5}$$

Where

$$\frac{1}{R} = \frac{1}{R_a} + \frac{1}{R_b} \tag{6}$$

The boundary conditions for the governing equations (1) and (2) are as follows:

$$u = U_1, \quad v=0 \qquad \text{at } y = 0 \tag{7}$$

$$u = U_2, \quad v=U_2 \frac{dh}{dX} \qquad \text{at } y = h \tag{8}$$

$$p=0 \quad \text{at} \quad x=-\infty$$

$$p=0 \quad , \frac{dp}{dx}=0 \qquad \text{at } x = x_2 \tag{9}$$

In order to solve the system of equations (1) and (2) for various bearing characteristics one has to first of all determine the sign of the velocity gradient $\frac{\partial u}{\partial y}$ i.e. to establish the regions of positive or negative velocity gradients. Particularly, in these areas no sharp changes have been observed in Newtonian fluid.

Equations (1) and (2) can be solved for n=1 and m to be a constant or a function of x-line, one can obtain [9]

$$u=U_1+(U_2-U_1)\frac{y}{h} - \left(\frac{y}{h}\frac{dp}{dx}\right)(h-y) \tag{10}$$

$$\frac{dp}{dX} = \frac{6(U_1+U_2)m(h-h_1)}{h^3} \tag{11}$$

It can be seen that u is a linear function of y at point where $\frac{dp}{dx} = 0$. At this point, the velocity gradient $\frac{\partial u}{\partial y} = \frac{(U_2-U_1)}{h}$, which can never be equal to zero, since$U_2 \neq U_1$. It can also be seen from fig. (2) that for each X, $\frac{\partial u}{\partial y}$ can vanish at only one point of Y (= δ) in the region
$-\infty \leq X \leq -X_1$and $-X_1 \leq X \leq -X_2$. Thus, these regions can be divided into four sub-regions separated by δ-profile, as shown in Fig. (2).

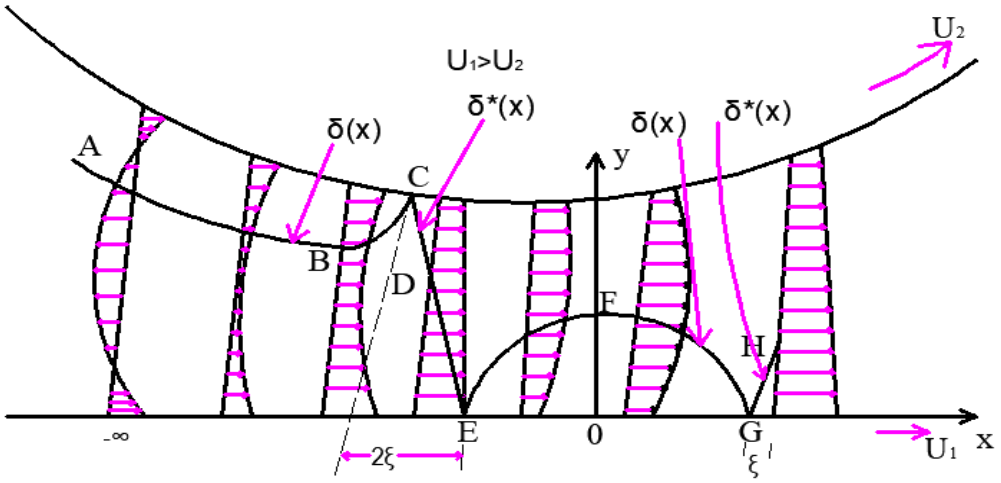

Fig. 2 Velocity profiles by arrow mark, δ- profiles by ABC and EFG, and δ*- profiles by CD, DE and GH, D being the middle point of height of the film thickness at X = X_1.

Let u_1, u_2 and u_3, u_4 be the velocities in the respective regions (see fig. (2.2)), then according to the velocity profile, shown in the figure, one may observe the following

$$\left.\begin{aligned}&\frac{\partial u_1}{\partial y}\geq 0, \delta \leq Y \leq h\\&\frac{\partial u_2}{\partial y}\leq 0, 0 \leq Y \leq \delta\\&\frac{\partial u_1}{\partial y}=\frac{\partial u_2}{\partial y}=0 \text{at}, Y=\delta\end{aligned}\right] -\infty \leq X \leq X_1 \tag{12}$$

$$\left.\begin{aligned}&\frac{\partial u_3}{\partial y}\geq 0, \delta \leq Y \leq h\\&\frac{\partial u_4}{\partial y}\leq 0, 0 \leq Y \leq \delta\\&\frac{\partial u_4}{\partial y}=\frac{\partial u_3}{\partial y}=0 \text{at}, Y=\delta\end{aligned}\right] -\infty \leq X \leq X_1 \tag{13}$$

It is expected that the nature of the velocity profiles for different n as well as variable m may remain unchanged but δ will certainly differ in each case.

Using the sign for the velocity gradients given in (12) and integrating equation (1) for the region $\delta \leq Y \leq h$, one can obtain

$$\frac{\partial u_1}{\partial y}=\left(\frac{1}{m_1}\frac{dp_1}{dx}\right)^{1/n}(y-\delta)^{1/n}$$

Further integration of this, using condition

$$u_1=u_2-\left(\frac{n}{n+1}\right)\left(\frac{1}{m_1}\frac{dp_1}{dx}\right)^{1/n}\left\{(h-\delta)^{n+1/n}-(y-\delta)^{n+1/n}\right\} \tag{14}$$

Similarly for the other regions, the following expressions can be obtained:

$$u_2=u_1-\left(\frac{n}{n+1}\right)\left(\frac{1}{m_1}\frac{dp_1}{dx}\right)^{1/n}\left\{\delta^{n+1/n}-(\delta-y)^{n+1/n}\right\} \tag{15}$$

$$u_3=u_1-\left(\frac{n}{n+1}\right)\left(-\frac{1}{m_2}\frac{dp_2}{dx}\right)^{1/n}\left\{\delta^{n+1/n}-(\delta-y)^{n+1/n}\right\} \tag{16}$$

$$u_4=u_2-\left(\frac{n}{n+1}\right)\left(-\frac{1}{m_2}\frac{dp_2}{dx}\right)^{1/n}\left\{(h-\delta)^{n+1/n}-(y-\delta)^{n+1/n}\right\} \tag{17}$$

Now the volume flux Q for the region $(-\infty \leq X \leq -X_1)$ is obtained as

$$Q=\int_0^h UDY \qquad \text{or} \quad Q=\int_0^\delta u_2 dy+\int_\delta^h u_1 dy$$

$$Q=u_1\delta+u_2(h-\delta)-\left(\frac{n}{2n+1}\right)\left(\frac{1}{m_1}\frac{dp_1}{dx}\right)^{1/n}\left\{\delta^{2n+1/n}+(h-\delta)^{2n+1/n}\right\} \tag{18}$$

Since the flux Q is constant through every cross section, thus the flux Q may be equated to the flux through the point X= -X_1 [10]. This point is selected in order to enforce the continuity of flow.

The flux Q through the point X = -X_1 (where $\frac{dp}{dx}=0$) can be evaluated directly from the equation (1), yielding

$$Q(x_1)=\frac{(u_1+u_2)}{2}h_1 \tag{19}$$

Finally equating the fluxes given by (18) and (19) and simplifying, one can obtain the following Reynolds equ

$$\left(\frac{dp_1}{dx}\right)=m_1(2n+1)^n\left[\frac{(u_1-u_2)\delta+u_2h-\left(\frac{u_1+u_2}{2}\right)h_1}{\delta^{2n+1/n}+(h-\delta)^{(2n+1)/n}}\right]^n,-\infty\le X\le -X_1 \tag{20}$$

Similarly for the other region, the Reynolds equation may be written as

$$\left(\frac{dp_2}{dx}\right)=m_2\left(\frac{2n+1}{n}\right)^n\left[\frac{(\frac{u_1+u_2}{2})h_1-u_2h-(u_1-u_2)\delta}{\delta^{2n+1/n}+(h-\delta)^{(2n+1)/n}}\right],-X_1\le X\le X_2 \tag{21}$$

Use of the matching conditions:

$$\left.\begin{matrix}u_1=u_2\\u_3=u_4\end{matrix}\right]\text{at}Y=\delta \tag{22}$$

Into (14-17) yields

$$u_2-u_1-\left(\frac{n}{n+1}\right)\left(\frac{1}{m_1}\frac{dp_1}{dx}\right)^{1/n}\left\{(h-\delta)^{(n+1)/n}-\delta^{(n+1)/n}\right\}=0,-\infty\le X\le X_1 \tag{23}$$

$$u_2-u_1-\left(\frac{n}{n+1}\right)\left(-\frac{1}{m_2}\frac{dp_2}{dx}\right)^{1/n}\left\{(h-\delta)^{(n+1)/n}-\delta^{(n+1)/n}\right\}=0,X_1\le X\le X_2 \tag{24}$$

Eliminating $\frac{dp_1}{dx}$ and $\frac{dp_2}{dx}$ from equations (23) and (24), using Reynolds equations (20) and (21), one can obtain a single relation as follows:

$$u_2-u_1-\left(\frac{2n+1}{n+1}\right)\frac{\left\{(h-\delta)^{(n+1)/n}-\delta^{(n+1)/n}\right\}\left\{(u_1-u_2)\delta+u_2h-\left(\frac{u_1+u_2}{2}\right)h_1\right\}}{\left[\delta^{(n+1)/n}+(h-\delta)^{(2n+1)/n}\right]}=0 \tag{25}$$

It must be noted here that the equation (25) cannot be used to evaluate δ at X = X_1 and X = X_2 since $\frac{\partial u}{\partial y}\neq 0$ there.

Energy Equation:

$$\frac{\partial^2T}{\partial Y^2}=-\left(\frac{m}{k}\right)\left|\frac{\partial u}{\partial y}\right|^{n-1}\left(\frac{\partial u}{\partial y}\right)^2 \tag{26}$$

Where the heat of convection has been neglected, The boundary conditions for this equation are

$$\begin{aligned}T&=T_o \quad \text{at } Y=0\\T&=T_h \quad \text{at } Y=h\end{aligned} \tag{27}$$

Integration of equation (26) twice for the region, $-\infty \le X \le -X_1$, gives

$$T_{11}=-\frac{n^2}{(2n+1)(3n+1)}\left(\frac{m_1}{k}\right)\left(\frac{1}{m_1}\frac{dp_1}{dx}\right)^{(n+1)/n}(Y-\delta)^{3n+1/n}+C_1Y+d_1 \tag{28}$$

$$T_{12}=-\frac{n^2}{(2n+1)(3n+1)}\left(\frac{m_1}{k}\right)\left(\frac{1}{m_1}\frac{dp_1}{dx}\right)^{(n+1)/n}(\delta-Y)^{3n+1/n}+C_2Y+d_2 \tag{29}$$

Where $T_{11}$and T_{12} are the lubricant temperature in the regions $\delta \le Y \le h$ and $0\le Y \le \delta$ respectively C_1, d_1 and C_2, d_2 are the integration constants. Use of the temperature matching condition

$T_{11} = T_{12}$ at $Y = \delta$ and the matching heat flux $k\frac{\partial T_{11}}{\partial Y} = k\frac{\partial T_{12}}{\partial Y}$ at $Y=\delta$

Implies

$C_1 = C_2 = C$ (say)

$d_1 = d_2 = d$ (say)

The constants C and d are evaluated using the boundary conditions (27) and are given below:

$$C = \frac{T_h - T_{o1}}{h} + \left(\frac{m_1 A_n}{hk}\right)\left(\frac{1}{m_1}\frac{dp_1}{dx}\right)^{(n+1)/n}\left[(h-\delta)^{(3n+1)/n} - \delta^{(3n+1)/n}\right] \quad (30)$$

$$d = T_{o1} + \left(\frac{m_1 A_n)}{k}\right)\left(\frac{1}{m_1}\frac{dp_1}{dx}\right)^{(n+1)/n}\delta^{(3n+1)/n} \quad \text{Where,} \quad A_n = \frac{n^2}{(2n+1)(3n+1)}$$

Thus, T_{11} and T_{12} are explicitly known functions of X and Y, giving temperature distribution in the region under consideration. Finally, the mean temperature T_{m_1}, as defined in equation (4), may be written as

$$T_{m1} = \frac{1}{h}\int_0^h T dy \qquad \text{or } T_{m1} = \frac{1}{h}\left[\int_0^\delta T_{12} dy + \int_\delta^h T_{11} dy\right]$$

$$\text{or } T_{m1} = \frac{T_h + T_{o1}}{2} + \frac{S_1}{2}\left[(h-\delta)^{(3n+1)/n} + \delta^{(3n+1)/n}\right] - \frac{nS_1}{(4n+1)h}\left\{(h-\delta)^{(4n+1)/n} + \delta^{(4n+1)/n}\right\} \quad (31)$$

Where

$$S_1 = \left(\frac{m_1 A_n}{k}\right)\left(\frac{1}{m_1}\frac{dp_1}{dx}\right)^{(n+1)/n} \quad (32)$$

Proceeding in the same way, the mean temperature for the region $-X_1 \le X \le X_2$, can also be written as

$$\text{or } T_{m2} = \frac{T_h + T_{o1}}{2} + \frac{S_2}{2}\left[(h-\delta)^{(3n+1)/n} + \delta^{(3n+1)/n}\right] - \frac{nS_2}{(4n+1)h}\left\{(h-\delta)^{(4n+1)/n} + \delta^{(4n+1)/n}\right\} \quad (33)$$

Where

$$S_2 = \left(\frac{m_2 A_n}{k}\right)\left(\frac{1}{m_2}\frac{dp_2}{dx}\right)^{(n+1)/n} \quad (34)$$

Using the non-dimensional scheme given with the following:

$$\overline{T_m} = T_m, \ \bar{\delta} = \frac{\delta}{h_o}(U), \ \bar{U} = \frac{U_1}{U_2} \ U_1 > U_2 \quad (35)$$

Equations (20), (21), (25), (31), (33) may be written as

$$\frac{d\bar{p}}{dx} = \bar{m}_1 \left(\bar{f}_x\right)^n \quad (36)$$

$$\frac{d\bar{p}_2}{dx} = -\bar{m}_2 \left(-\bar{f}_x\right)^n \quad (37)$$

$$1-\bar{U}\left(\frac{2n+1}{n+1}\right)\frac{\left\{\left(H-\bar{\delta}\right)^{(n+1)/n} - \bar{\delta}^{(2n+1)/n}\right\}\left\{\left(\bar{U}-1\right)\bar{\delta} + H - \left(\frac{1+U}{2}\right)H_1\right\}}{\left[\bar{\delta}^{(2n+1)/n} + \left(H-\bar{\delta}\right)^{(2n+1)/n}\right]} = 0 \quad (38)$$

$$\bar{T}_{m1} = \frac{\bar{T}_n + \bar{T}_{o1}}{2} + \bar{m}_1 d_n \bar{\gamma}_s \left(\bar{f}_n\right)^{n+1} \bar{g}_x \quad (39)$$

$$\bar{T}_{m2} = \frac{\bar{T}_n + \bar{T}_{o1}}{2} + \bar{m}_2 d_n \bar{\gamma}_s \left(-\bar{f}_n\right)^{n+1} \bar{g}_x \tag{40}$$

Where

$$\bar{m}_1 = \bar{m}_o \; e^{\bar{p}_1 - \bar{T}_{m1} + \bar{T}_o}, \bar{m}_2 = \bar{m}_o \; e^{\bar{p}_1 - \bar{T}_{m1} + \bar{T}_o} \tag{41}$$

$$\bar{\gamma}_s = \left(\frac{U_2 h_o \beta}{k\alpha}\right)\left(\frac{h_o}{2R}\right)^{1/2} \tag{42}$$

$$d_n = \frac{n}{(3n+1)\; 2^{(n+1)}} \tag{43}$$

$$\bar{f}_X = \left[\frac{\left(\bar{U}\text{-}1\right)\bar{\delta} + H - \left(\frac{1+\bar{U}}{2}\right)H_1}{\bar{\delta}^{(2n+1/n)} + \left(H - \bar{\delta}\right)^{(2n+1)/n}}\right] \tag{44}$$

$$\bar{g}_x = \frac{1}{2}\left\{\left(H\text{-}\bar{\delta}\right)^{(3n+1)/n} + \bar{\delta}^{(3n+1)/1}\right\} - \frac{n}{(4n+1)H}\left\{\left(H\text{-}\bar{\delta}\right)^{(4n+1)/n} + \bar{\delta}^{(4n+1)/1}\right\} \tag{45}$$

Equations (36), (39) and (37) have to be solved simultaneously using the following conditions:

$$\bar{P}_1 = 0 \text{ at } X = -\infty \tag{46}$$

$$\left.\begin{aligned} \bar{P}_2 &= 0 \\ \frac{d\bar{p}_2}{dx} &= 0 \end{aligned}\right| \text{at} X = X_2 \tag{47}$$

From equation (37), it may be observed that the condition

$$\frac{dP_2}{dX} = 0 \text{ at } X = X_2 \text{ Implies}$$

$$\left(\bar{U}\text{-}1\right)\bar{\delta}_2 + H_2 - \frac{\left(\bar{U}+1\right)}{2}H_1 = 0 \tag{48}$$

Since $\bar{\delta}_2$ comes out to be $H_2/2$ (for detail, see numerical calculation, section (2.3)). It follows that

$$X_2 = X_1 \tag{49}$$

Thus $X = X_1$ gives the point of cavitation.

3. RESULTS AND DISCUSSION

Numerical solutions of the Reynolds equations (36, 37) and the energy equations (39, 40) have been obtained for anti-symmetric, viscous incompressible flow of a power law fluid through the gap between a cylinder and a plane (see Fig. 1). The results of this investigation are assumed in terms of parameters n and $\bar{U}$ ($= U_1/U_2$, $U_1 > U_2$). The values of n have already been mentioned in Table 1, 2, 3. The sliding parameters $\bar{U}$ is chosen to lie between 1 and 1.2 (i.e. max of 20% slip). The parameter $\bar{U}$ arises due to the consideration of anti-symmetric conditions and is important because the presence of sliding ($\bar{U} > 1$) is likely to yield more pressure and temperature as compared to that for pure rolling ($\bar{U} = 1$). The significance of $\bar{U}$ along with n has been demonstrated through Tables and graphs. For the numerical calculation, the following representative values have been used:

U_2 = 400 cm sec^{-1}, h_0 = 5x 10^{-4} cm, α = 1.6x 10^{-9} $dyne^{-1}$ cm^2, R = 3 cm, $\overline{T}_h = 1.5$, $\overline{T}_{01} = 1$. The thermal factor is $\bar{\gamma}_s = \left(U_2 h_o \beta \sqrt{\frac{h_o / 2R}{k\alpha}} \right)$ chosen to be 5.

An important feature of this problem is that this reduces to (a) the exact problem done in [11] for $U_1 = U_2$ and m = constant, (b) a similar problem done in [12] for n= 1.

3.1 Numerical Solutions: The Reynolds and energy equations are coupled through $\overline{m}$ and contain two unknowns $\bar{\delta}$ (the locus of points at which $\frac{\partial u}{\partial y} = 0$) and X_1 (X = -X_1 is the point of maximum pressure). These unknowns are also present in equation (38). As there is no symmetry ($\overline{U} \neq 1$) for $\bar{\delta}$ - distribution, it is necessary to solve equation (38) $\bar{\delta}$ over the complete region under consideration, along with Reynolds and energy equations. The actual process followed for the numerical calculations is given below. The algebraic equation (38) in $\bar{\delta}$ contains X and X_1 explicitly. First of all an initial value of X is assigned i.e. the point at minus infinity is replaced by a large but a finite negative value. An arbitrary value of X_1 is chosen. The value of $\bar{\delta}$ ay the inlet is obtained by solving the algebraic equation (38) for $\bar{\delta}$using the bisection method with a reasonable tolerance (say 10^{-4}). These value of X and $\bar{\delta}$ are substituted in the energy equation (39). $\overline{T}_{m_1}$ At the inlet is then obtained from solving the algebraic energy equation by prescribing $\overline{m}_0$ and $\bar{p}_1$ (=0 at $X = -\infty$) and using the earlier numerical technique. The same X, $\overline{m}_0$ and the computed $\bar{\delta}$ and $\overline{T}_{m_1}$ are used in the differential equation (4.36). Fourth order Runga-kutta method is used to evaluate $\bar{p}_1$ at X = X+ΔX. For this value of X (=X+ΔX), equation (38) is solved for $\bar{\delta}$. These new X, $\bar{\delta}$ and $\bar{p}_1$ are substituted in the energy equation which again yields$\overline{T}_{m_1}$. X and $\bar{\delta}$ are used to calculate $\bar{p}_1$ as a solution of equation (36) at another point X =X+2ΔX. This process is repeated for further values of X till such time that equation (4.38) yields values of $\bar{\delta}$ satisfying $0 \leq \bar{\delta} \leq H$ (because $\bar{\delta}$ cannot exceed H). It may be noted that at X = -X_1, $\bar{\delta}$ does not exist (see previous section). Further in the neighbor-hood (n-hood) of X = -X_1, the determined values of $\bar{\delta}$ do not lie in the interval $0 \leq \bar{\delta} \leq H$. Hence in the n'hood of X = -X_1, $\bar{\delta}$ (= say $\bar{\delta}^*$) has to be determined solely on the basis of physical consideration. It should be emphasized hear that $\bar{\delta}^*$ does not refer to the locus of points at which the velocity gradient vanishes. Let one consider a ∈ - n'hood $(-X_1 - \epsilon \leq X \leq -X_1 + \epsilon, \epsilon > 0)$ of the point X = X_1 where there exists no $\bar{\delta}$ lying in the interval $0 \leq X \leq H$ and satisfying equation (38). To ease the mathematical complexity, a linear profile for $\bar{\delta}$ given below

$$\overline{\delta^*}(X) = \frac{H}{2\epsilon}(X + X_1 - \epsilon) \qquad (50)$$

is assumed. This profile was chosen in such a manner that it not only satisfies the Reynolds equation atX = -X_1, but also make the pressure curve continuous. Having determined $\bar{\delta} = \bar{\delta}^*$ using equation (50) in the n'hood of the point X = -X_1, the procedure outlined earlier is adopted to evaluate $\bar{p}_1$ and $\overline{T}_{m_1}$for the region $-X_1 - \epsilon \leq X \leq -X_1$ and $\bar{p}_2$, $\overline{T}_{m_2}$ for the region $-X_1 \leq X \leq -X_1 + \epsilon$. Since in the interval $-X_1 + \epsilon \leq X \leq -X_1 - \epsilon$, $\bar{\delta}$ (roots of equation (4.38)) satisfies the inequality $0 \leq \bar{\delta} \leq H$, so $\bar{\delta}$ in the region $-X_1 + \epsilon \leq X \leq -X_1 - \epsilon$ is determined (by the same procedure followed near the inlet) along with $\bar{p}_2$ and $\overline{T}_{m_2}$.subsequently in the interval $-X_2 - \epsilon \leq X \leq X_2$. Since equation (38) is not valid at X = X_2), the same type of linear profile given below

$$\overline{\delta^*}(X) = \frac{H_2}{2\epsilon}(X - X_2 + \epsilon), -X_2 - \varepsilon \leq X \leq X_2 \qquad (51)$$

Is assumed (the complete $\bar{\delta}$ - profile has been shown in Fig. 2. This will satisfy the Reynolds cavitations boundary condition (47) i.e

$$\frac{d\bar{p}_2}{dx} = 0 \text{ at } X = X_2 \qquad (52)$$

if $X_2 = X_1$

$\bar{\delta}$ In the region $-X_1 - \epsilon \leq X \leq X_1$ is calculated using relation (4.48) together with $\bar{p}_2$ and $\overline{T}_{m_2}$. If the computed value of $\bar{p}_2$ at X = X_1 satisfies the condition (4.47) (i.e. $\bar{p}_2 = 0$ at X = X_1), the assumed arbitrary value of X_1 was correct. Otherwise another value of X_1 is assigned and the whole process is repeated as long as $\bar{p}_2$ vanishes at X = X_1. Thus X_1

and $\bar{\delta}$ (as a function of $X_o$are computed along with pressure $\bar{p}_1$, $\bar{p}_2$ and the mean temperature $\overline{T}_{m_1}$, $\overline{T}_{m_2}$. The complete pressure and the mean temperature profiles as functions of n and $\overline{U}$ have been presented in the following sections.

Creating an artificial intelligence (AI) model in MATLAB to analyze the thermal effects in lubrication of rolling involves several steps, including data collection, preprocessing, model selection, training, and validation. Below is a simplified example of how you might approach this problem using MATLAB:

1. **Data Preparation**: Gather and preprocess the data related to thermal effects and lubrication.
2. **Feature Selection**: Select relevant features for the model.
3. **Model Selection**: Choose an appropriate AI model (e.g., neural network, regression model).
4. **Training the Model**: Train the model using the prepared data.
5. **Validation and Testing**: Validate and test the model to ensure accuracy.

The code has been run through MATLAB software and the sample of the Artificial Intelligence Based PSEDUO coding is given below.

```
% Load and preprocess data
data = load('lubrication_data.mat'); % Assume data is in a .mat file
X = data.features; % Features for the model
y = data.targets; % Target variable (e.g., temperature or pressure)

% Split data into training and testing sets
[trainInd, valInd, testInd] = dividerand(size(X, 1), 0.7, 0.15, 0.15);
X_train = X(trainInd, :);
y_train = y(trainInd, :);
X_val = X(valInd, :);
y_val = y(valInd, :);
X_test = X(testInd, :);
y_test = y(testInd, :);
% Create and configure neural network
hiddenLayerSize = 10; % Number of neurons in hidden layer
net = fitnet(hiddenLayerSize);
% Set up division of data for training, validation, and testing
net.divideFcn = 'divideind';
net.divideParam.trainInd = trainInd;
net.divideParam.valInd = valInd;
net.divideParam.testInd = testInd;
% Train the network
[net, tr] = train(net, X_train', y_train');
% Test the network
y_pred = net(X_test');
% Calculate performance
performance = perform(net, y_test', y_pred);
% Plot results
figure;
plot(y_test, y_pred, 'o');
xlabel('True Values');
ylabel('Predictions');
title('Neural Network Predictions vs. True Values');
grid on;
% Save the trained network
Save ('trained_lubrication_net.mat', 'net');
```

Explanation of PSEUDO Code:

1. **Load and Preprocess Data**: Load the dataset and split it into features (X) and target variables (y).
2. **Data Splitting**: Divide the data into training, validation, and testing sets.
3. **Create and Configure Neural Network**: Define a neural network with a specified number of hidden layers and neurons. Set up the division of data for training, validation, and testing.
4. **Train the Network**: Train the neural network using the training data.
5. **Test the Network**: Test the trained network on the testing data and calculate performance metrics.
6. **Plot Results**: Plot the true values versus the predicted values to visualize the performance of the model.
7. **Save the Trained Network**: Save the trained network for future use.

Imperative Data for AI Based coding:

- **Data Preprocessing**: Depending on your data, you might need to perform additional preprocessing steps such as normalization or feature engineering.
- **Hyperparameter Tuning**: Adjust the number of hidden layers, neurons, and other hyperparameters to optimize the model.
- **Performance Metrics**: Use appropriate performance metrics (e.g., MSE, RMSE) to evaluate the model's accuracy.

3.2 Pressure Profile: The pressure profile $\bar{p}$ has been presented for various values on n and $\bar{U}$ in Fig. 3a and data given in Table 1. It can be seen that for each fixed n and $\bar{U}$. It can also be noted that for a fixed $\bar{U}$, the qualitative behavior of $\bar{p}$ with respect to n remains unaltered i.e. $\bar{p}$ increases with n. for a fixed n, $\bar{p}$ increases with $\bar{U}$. This can be seen through the Fig. 3 for values of $n \geq 1$. $\bar{p}$ Depicts the same trend for $n < 1$, also however it has not been shown because of overlap plying of curves. $\bar{p}$ Increases with $\bar{U}$ which implies that hydrodynamic pressure due to sliding is higher than that for the pure rolling. This is justified also because the rolling friction is always less than the sliding friction.

Table 1: Pressure distribution when n varies

Pressure distribution when n varies				
X	n=1.15	n= 1.0	n= 0.545	n= 0.4
-5	0.01	-	-	-
-4	0.016582	-	-	-
-3	0.027476	0.01	-	-
-2.3	0.039127	0.01281	0.01	-
-2	0.045527	0.014313	0.010373	-
-1.26	0.066156	0.018821	0.012453	0.01
-1	0.075438	0.020722	0.013279	0.01
-0.65	0.090023	0.023587	0.014478	0.0105
-0.55	0.094686	0.024476	0.014841	0.011
-0.5	0.097107	0.024933	0.015025	0.0125
0	0.125	0.03	0.0175	0.01
0.33	0	0	0	0

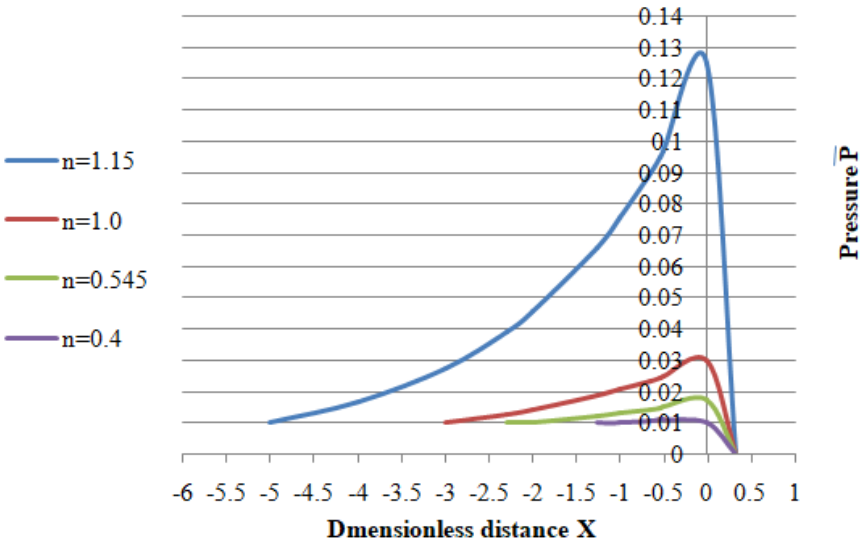

Fig. 3a Pressure distribution $\bar{P}$ vs X

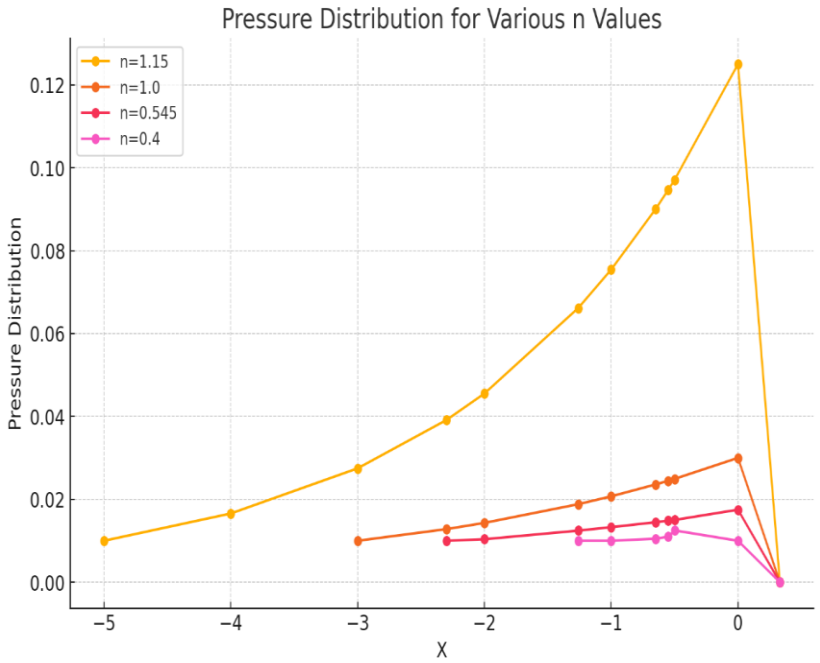

Fig. 3b Graphical representation of pressure distribution $\overline{P}$ vs X

Here Fig. 3b shows the graph showing and Fig. 3c shows the AI based bar graph pressure distribution for various n values. The graph plots the pressure distribution against X for n=1.15, n=1.0, n=1.15, n=0.545, n =0.4. The markers indicate the given data points, and the lines connect these points to visualize the trends.

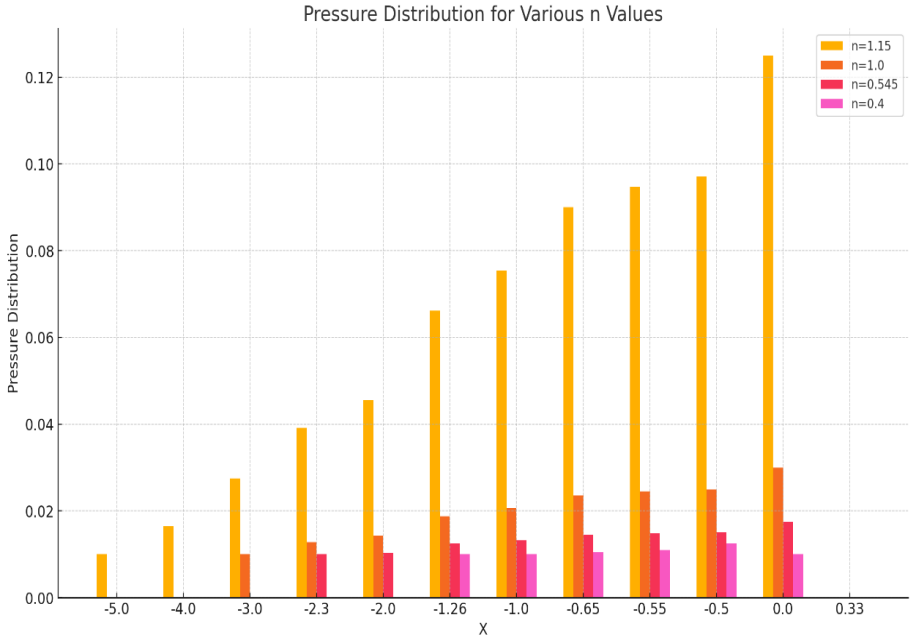

Fig. 3c AI Based BAR graph representation of pressure distribution $\overline{P}$ vs X

3.3 Temperature Profile: The mean temperature distribution has been depicted in Fig. 4a as a function of n and $\overline{U}$ and data given in Table 2. For a fixed $\overline{U}$, $\overline{T}_m$ increases with increasing value of n. This pattern also is in accordance with the results mentioned in this current study (for q = 0). For a fixed n, $\overline{T}_m$ increases with $\overline{U}$ (its behavior is similar to that of the pressure profile). Hence the same geometrical interpretation may follow here. It may be easily concluded that the sliding temperature is higher than for the pure rolling.

Table 2: Temperature distribution when n varies

Temperature distribution when n varies				
X	n=1.15	n= 1.0	n= 0.545	n= 0.4
-5	2.172500611	1.51099	1.351636	1.260069
-4	2.076285996	1.487572	1.342918	1.259226
-3	1.958504669	1.457915	1.331761	1.25814
-2	1.803757233	1.417118	1.316193	1.25661
-1	1.567	1.35	1.29	1.254
-0.33	1.25	1.25	1.25	1.25
-0.27	1.2884344	1.261599	1.258306	1.256315
-0.12	1.3506784	1.280378	1.271702	1.266494
0	1.366	1.285	1.275	1.269
0.12	1.3506784	1.280378	1.271702	1.266494
0.27	1.2884344	1.261599	1.258306	1.256315
0.33	1.25	1.25	1.25	1.25

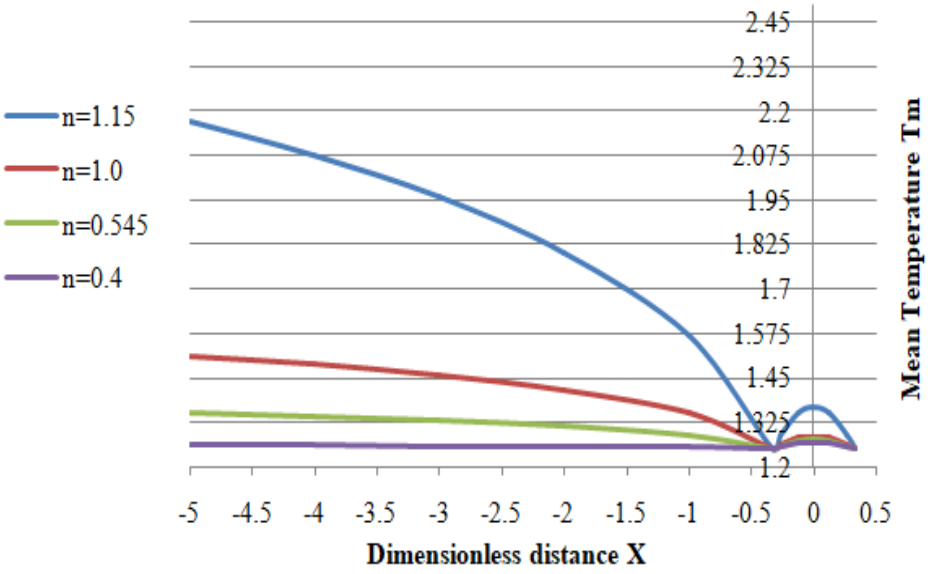

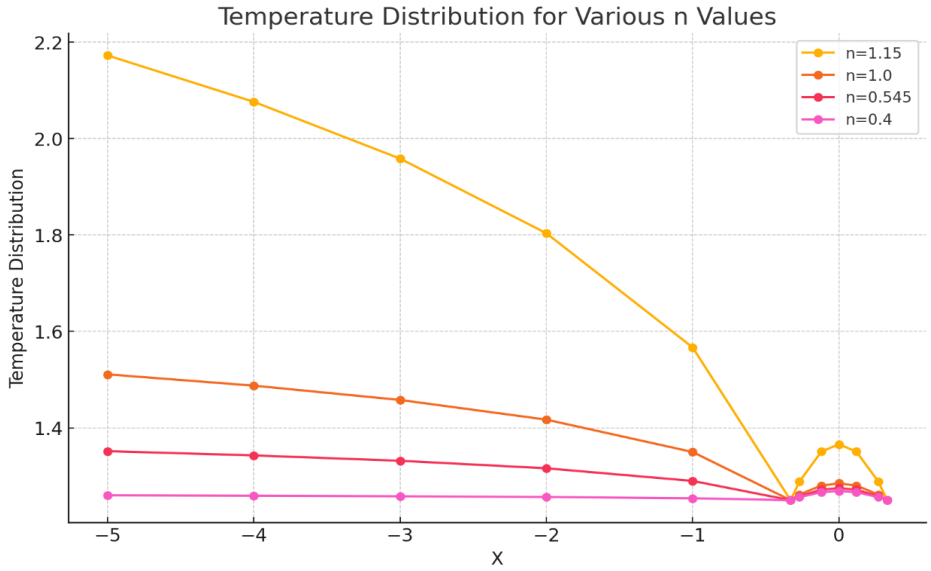

Fig. 4b Graphical representation of the mean temperature distribution $\overline{T}_m$ vs X by AI

Here Fig. 4b shows the graphical representation and Fig. 4c shows the AI based bar graph of temperature distribution for various n values. The graph plots the temperature distribution against X for n=1.15, n=1.0, n=1.15, n=0.545, n =0.4. The markers indicate the given data points, and the lines connect these points to visualize the trends.

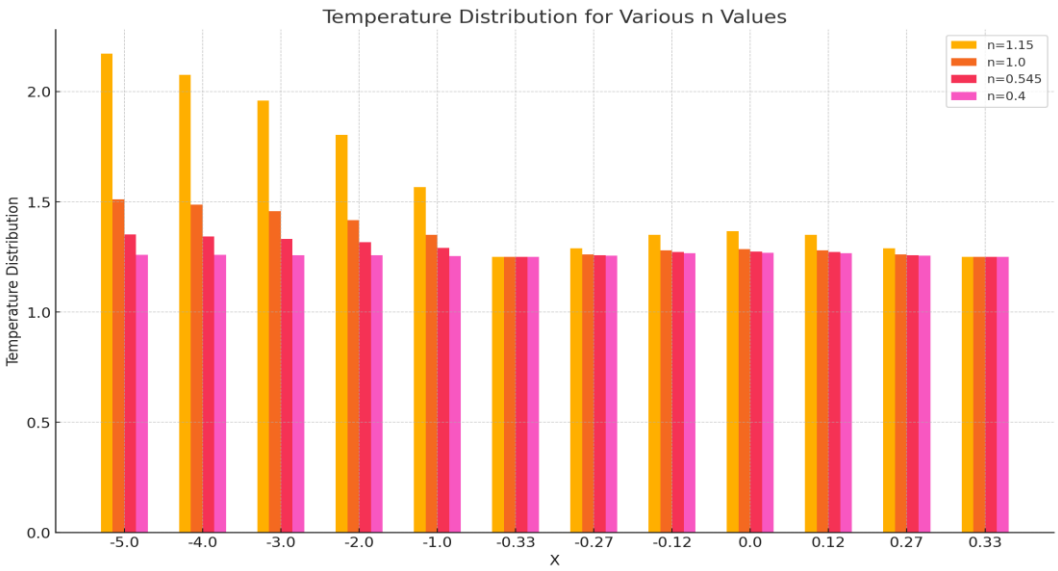

Fig. 4c AI Based BAR graph representation of the mean temperature distribution $\overline{T}_m$ vs X by AI

3.4 Consistency Profile: The characteristic behavior of the Consistency $\overline{m}$ i.e. over all change in $\overline{m}$ due to the combined effect of pressure $\overline{p}$ and the temperature $\overline{T}_m$ (see relation (41)) has been demonstrated $\overline{m}$ versus X is qualitatively almost similar to the pressure profile depicted in Fig. 5a and data given in Table 3. The difference appears (in case of $n > 1$) near the inlet as well as outlet. However, $n \leq 1$, the difference appears only near the outlet. Near the inlet (for $n > 1$), $\overline{m}$ decreases because the increase in $\overline{p}$ is unable to compensate for the temperature rise. After that it is almost flattened because of equal contribution of $\overline{p}$ and $\overline{T}_m$ .Again at the outlet for all n) $\overline{m}$ increases (through very marginal) since the impact of the reduced temperature is higher than that of the reduced pressure. Further the consistency peak in the low-pressure gradient region is quite sharp. This happens due to sharp increase in $\overline{p}$ and decrease in $\overline{T}_m$ (when $X \neg X_1$) simultaneously. For a fixed $\overline{U}$, $\overline{m}$ increases with n. similarly for a fixed $(n > 1)$, it increases with $\overline{U}$ expect near the inlet where the trend is reversed. For a fixed $n \leq 1$, a similar trend has been obtained, however it has not be shown due to overlapping of curves.

Table 3: Consistency distribution when n varies

Consistency distribution when n varies				
X	n=1.15	n= 1.0	n= 0.545	n= 0.4
-5	0.68	0.2	0.08	0.04
-4	1.117298	0.24987	0.097048	0.04
-3	1.831094	0.313858	0.115839	0.04
-2	3.000904	0.394232	0.138269	0.04
-1	4.918057	0.495189	0.165043	0.04
-0.5	6.32	0.56	0.18	0.04
0	2.76	0.44	0.12	0.04
0.3	2.25	0.36	0.1	0.04
0.5	2.32	0.4	0.08	0.04

Here Fig. 5b shows the graphical representation and Fig. 5c shows the AI based bar graph of consistency distribution for various n values. The graph plots the consistency distribution against X for n=1.15, n=1.0, n=1.15, n=0.545, n =0.4. The markers indicate the given data points, and the lines connect these points to visualize the trends.

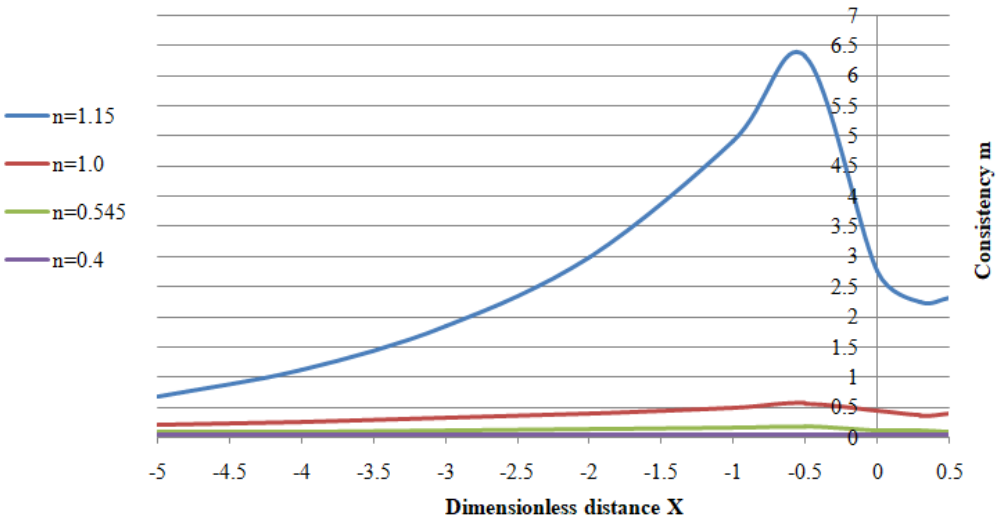

Fig. 5a Consistency distribution $\bar{m}$ vs X

Fig. 5b Graphical representation of the consistency distribution $\bar{m}$ vs X using AI

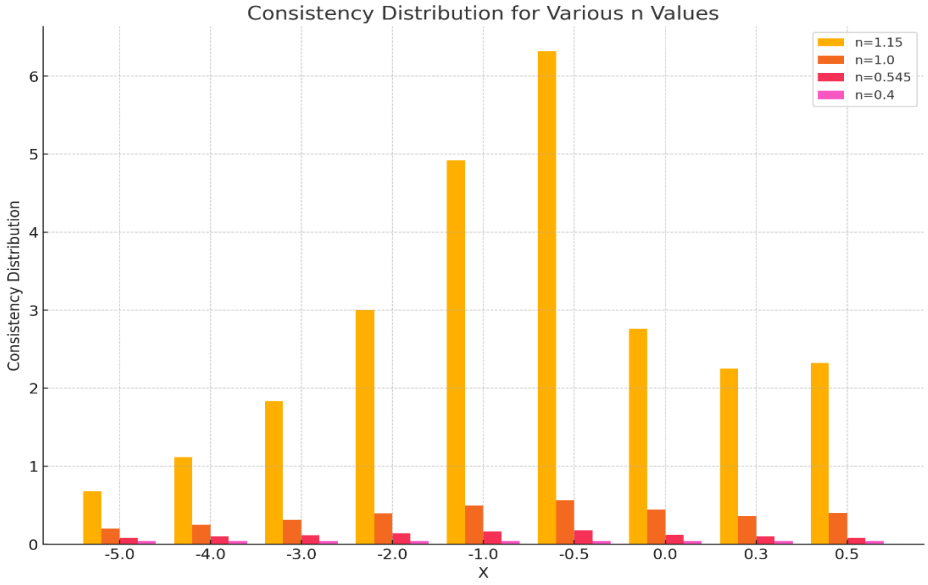

Fig. 5c AI Based BAR graph representations of the consistency distribution $\bar{m}$ vs X

4. CONCLUSIONS

In the present study, the impact of thermal effects of non-Newtonian fluids in lubrication of rollers in rolling or sliding contacts has been studied well in both uniform and non-uniform conditions using standard mathematical tools. The physical characteristic of fluid which follows power law has been studied well. The following conclusions have been derived from the present study:

(a) The increase in pressure (hence the load and traction) with flow index n for a fixed value of $\overline{U}$. A similar trend follows when $\overline{U}$ is varied (from 1 to 1.2) and n is held fixed.

(b) The variation in the avg. temperature with respect to $\overline{U}$and n were satisfied up to some extent.

(c) Apart from that, the consistency variation resulting from $\overline{p}$ and $\overline{T}_m$ is significant. Especially the curve trends are quite better in the peak region of pressure for dilatants fluids and Newtonian.

5. REFERENCES

1. Hirst W. and Lewis, M.G., "The rheology of oils during impact" Proc. Roy. Soc. London, Ser. A334 (1973)1.
2. Sinha, P. and Singh C., "Lubrication of cylinder on a plan with a non-Newtonian fluid containing additives and contaminants" Wear, 81 (1982)33.
3. Sinha, p., Shukla, J.B, Singh, C. and Prasad, K.R., "non-Newtonian lubrication theory for rough surfaces application to rough and elastic rollers" J. Mech. Engr. Sci., 24 (1982)147.
4. Sinha, P. and Raj, A. "Exponential viscosity variation in the non-Newtonian lubrication of rollers considering cavitation" wear, 87 (1983) 29.
5. Sinha, P., Shukla, J.B., Prasad, K.R. and Sinha, C., "non-Newtonian power law fluid lubrication of lightly loaded cylinders with normal and rolling motion" wear, 89 (1983)313.
6. Salem, E.A. , Khalil , M.F. and Bedewi, M.A., "Thermal and inertia effects in externally pressurized spherical bearings lubricated with non-Newtonian fluids" wear, 91(1983)15.
7. Bush, A.W., Hughes, G.D. and Skinner, P.H., "The influence of surface roughness and non-Newtonian effects in elasto hydrodynamic lubrication" presented at 10th Leeds/Nyon Symposium on Tribology, Leeds 1984.
8. Rodkiewicz, C.M. and Srinivasan, V., "EHL in rolling and sliding contacts" J.Lub. Tech., 94(1972)324.
9. Cheng, H. S.and Sternlicht, B. "A numerical solution for pressure temperature and film thickness between two infinitely long lubricated rolling and sliding cylinders,under heavy loads" J. Basic Engr.87 (1965) 695.
10. Shew, S. and Wilsion, W.R.D., "viscoplastic lubrication of asperities" J. Lub. Tech., 104(1982)568.
11. Safar, Z.S., "Journal bearing operating with non-Newtonian lubricating films" wear, 53 (1979) 95.
12. Pascovici, M.D., "Temperature distribution in lubricant film of slider bearing under intensive lubricant wall heat transfer conditions" Wear, 29 (1974) 227.